

Article

# A New Sliding-Mode Observer-Based Deadbeat Predictive Current Control Method for Permanent Magnet Motor Drive

Zixuan Zhang<sup>1</sup>, Qiangren Xu<sup>2,\*</sup> and Yicheng Wang<sup>2</sup> 

<sup>1</sup> Zhejiang University–University of Illinois Urbana-Champaign Institute, Haining 314400, China; zixuanz.21@intl.zju.edu.cn

<sup>2</sup> School of Electrical Engineering, Southeast University, Nanjing 210096, China; 230218324@seu.edu.cn

\* Correspondence: 230228743@seu.edu.cn

**Abstract:** This article proposes a new deadbeat predictive current control (DPCC) method based on a sliding-mode observer (SMO), which is applied in the field of permanent magnet motor control. A novel DPCC control method based on SMO is proposed according to the inherent issues of DPCC, which can effectively suppress internal parameter mismatch disturbances and external disturbances in the current loop. The mathematical model and derivation process of the proposed method are introduced. A simulation model is built and the effectiveness of the proposed method is verified. An experimental platform is built and the superiority of the proposed method is verified based on comparative experiments. Experimental results show that the proposed algorithm has strong robustness to the motor parameter mismatch. Compared with extended state observer (ESO) and adaptive observer (AO), the proposed algorithm has faster response speed and higher steady-state accuracy.

**Keywords:** deadbeat predictive current control; sliding-mode observer; permanent magnet; motor control



**Citation:** Zhang, Z.; Xu, Q.; Wang, Y. A New Sliding-Mode Observer-Based Deadbeat Predictive Current Control Method for Permanent Magnet Motor Drive. *Machines* **2024**, *12*, 297.

<https://doi.org/10.3390/machines12050297>

Received: 15 March 2024

Revised: 21 April 2024

Accepted: 23 April 2024

Published: 28 April 2024



**Copyright:** © 2024 by the authors. Licensee MDPI, Basel, Switzerland. This article is an open access article distributed under the terms and conditions of the Creative Commons Attribution (CC BY) license (<https://creativecommons.org/licenses/by/4.0/>).

## 1. Introduction

In the present era of low-carbon demand, electric transportation propelled by permanent magnet motors has emerged as a prominent area of research [1]. The motor serves as the fundamental component of electric transport vehicles. With its uncomplicated design, high power density, and straightforward controllability, the permanent magnet synchronous motor (PMSM) stands out as a prime selection among permanent magnet motors [2].

Enhancing motor control precision and reliability is imperative for ensuring the safe and stable operation of electric transportation devices [3]. The efficacy of motor control hinges on the adopted current control methodology [4]. To swiftly and accurately track current, several advanced current control techniques have been explored and implemented. Among these, hysteresis current control [5,6], pulse width modulation control [7,8], and predictive current control (PCC) [9,10] stand out as exemplary methods. Electric transport motor systems encounter diverse steady-state and dynamic scenarios. Irrespective of the environment, the primary objective of current control remains consistent: maintaining stator current stability and adeptly tracking its reference. PCC, by leveraging optimal voltage vectors, mitigates stator current errors and optimally fulfills the objective of current control.

Currently, three approaches exist for implementing PCC. The first approach is a finite control set PCC [11]. This method involves predicting the motor's state resulting from each potential optimal voltage vector of the inverter, thereby markedly enhancing motor control accuracy. In [12], a novel finite control set PCC method is introduced, offering a more readily implementable means to achieve optimal control by compensating for fluctuating currents and selecting the optimal switching state for each cycle. In [13], enhancements were made to the current change update mechanism of the limited control set PCC. Leveraging the super local model, the update frequency of the current was augmented, enabling the

selection of the optimal voltage vector with minimal cost function. Nonetheless, as the prediction range expands and prediction times lengthen, the control efficacy becomes subject to limitations imposed by the microcontroller's computing performance [3].

The second approach to implementing PCC builds upon the first, refining its methodology. Unlike expanding the prediction range, this method focuses on broadening the search and utilization of the optimal voltage vector [14]. In [15], an enhanced bidirectional predictive current control method is introduced, employing an active vector in lieu of a zero vector. This approach establishes a vector selection table by testing the control system to identify the optimal vector combination across various conditions. Reference [16] concurrently utilizes both active voltage and zero vectors. By calculating the optimal timing for different voltage vectors based on the  $q$ -axis current slope, this method reduces the current ripple by determining the timing of the active and zero vectors. Despite advancements in control performance, these methods still encounter limitations in computing performance.

The third approach, deadbeat predictive current control (DPCC), relies on a discrete model to forecast the optimal voltage vector. This method enables direct acquisition of the optimal voltage vector through a single calculation, thereby eliminating errors within one control cycle [17]. Achieving precise tracking necessitates the controller to swiftly adjust the system output. This entails a larger gain to amplify the error signal and expedite system state adjustments. Parameter mismatches prompt the controller to increase the gain for compensation. However, the heightened sensitivity to high-frequency noise and rapid response speed diminishes the phase margin. In [18], a novel DPCC method is introduced, enhancing the primary control loop by integrating a combination of super distortion algorithms to bolster DPCC's control performance. Another variant, M-DPCC, is proposed in [3], extending single-step prediction to the entire dynamic range under transient conditions and enabling multi-step deadbeat calculations, thereby comprehensively optimizing stator voltage vector angles. While DPCC boasts superior control accuracy, it may be susceptible to internal motor parameters, leading to diminished control efficacy [19]. External disturbances commonly encountered by permanent magnet motors can also impact DPCC, which relies heavily on environmental factors, thus affecting control performance.

Observer-based control methods, adept at compensating for the influences of unknown disturbances and uncertain model parameters in motion control systems [20], serve to bolster the robustness of the entire control system without compromising its original performance [21]. Among the array of observer-based control methods are adaptive observers [22,23], active disturbance rejection observers [24,25], and sliding-mode observers [26], among others. While the adaptive observer exhibits commendable control efficacy against summarized disturbances, it is prone to constraint by the controller's own control law, thereby diminishing its capacity to reject unknown disturbances. Active disturbance rejection control, on the other hand, demonstrates notable suppression of both internal and external disturbances. However, its intricate structure and multitude of internal control parameters pose challenges in achieving optimal control performance. Moreover, the disturbances encountered by permanent magnet motors often manifest as continuous fluctuations, whereas most observers assume them to be constant, thereby constraining their actual effectiveness.

Sliding-mode control, a strategy within variable structure control systems [27], utilizes sliding-mode control observers (SMOs) characterized by insensitivity to disturbances and parameters. SMOs offer notable advantages, including robust disturbance rejection and rapid response [28]. Hence, this paper proposes an enhanced DPCC control method for permanent magnet motors, amalgamating the strengths of DPCC and SMOs while refining DPCC's control performance. A prevalent approach to enhancing control system performance is robustness design, aimed at mitigating high control gains and augmenting phase margin. Through the adoption of robust design methodologies, the adverse impact of elevated control gains on system stability can be alleviated to a certain extent.

Several improvement measures have been proposed for DPCC by researchers, yet limitations persist. The adaptive observer may be constrained by the controller's control law,

thereby diminishing its ability to reject unknown disturbances. Additionally, the complex structure and numerous internal control parameters pose challenges to achieving optimal control performance with active disturbance rejection control. This paper endeavors to enhance DPCC from a novel standpoint.

To address the deficiencies of parameter sensitivity, limited robustness, and compromised system stability within DPCC, this paper introduces a novel approach employing a robust and straightforward SMO to counteract performance degradation resulting from parameter mismatches and external disturbances. Notably, this approach offers simplicity of implementation without significantly increasing computational overhead. Through simulation and experimental validation, it demonstrates superior performance compared to alternative algorithms, thus presenting significant potential for practical application.

The structure of this article is as follows: In Section 2, the basic equations of PMSM are introduced and a mathematical model of DPCC is built based on it. In Section 3, a slide-mode observer is designed based on DPCC, and a novel DPCC algorithm based on SMO is formed. In Sections 4 and 5, simulations and experimental tests are conducted to verify the effectiveness and superiority of the proposed method.

## 2. Mathematical Model of PMSM and DPCC

### 2.1. Mathematical Model of PMSM

With the following assumptions in [29], the motor operates without considering spatial harmonics and core losses. Assuming symmetry in the three-phase windings of the stator, the magnetomotive force generated is distributed in a sinusoidal pattern along the air gap. Neglecting magnetic circuit saturation, the self-inductance and mutual inductance of each winding remain constant. Additionally, the impact of frequency and temperature variations on the winding resistance is disregarded. In a synchronous rotating coordinate system, the mathematical model of PMSM can be represented as follows:

$$\begin{cases} \dot{i}_d = -\frac{R}{L}i_d + n_p\omega_m i_q + \frac{1}{L}u_d \\ \dot{i}_q = -\frac{R}{L}i_q - n_p\omega_m i_d + \frac{1}{L}u_q - \frac{1}{L}n_p\omega_m\psi_f \\ J\dot{\omega}_m = T_e - B\omega_m - T_L \\ T_e = \frac{3}{2}n_p\psi_f i_q \end{cases} \quad (1)$$

where  $u_d$  and  $u_q$  are the  $d$ - and  $q$ -axis stator voltages, respectively;  $i_d$  and  $i_q$  are the  $d$ - and  $q$ -axis stator currents, respectively;  $L_d$  and  $L_q$  are  $d$ - and  $q$ -axis inductances, respectively, and  $L = L_d = L_q$ .  $T_e$  is the electromagnetic torque,  $T_L$  is the load torque,  $\omega_m$  is the mechanical angular velocity,  $n_p$  is the number of pole pairs,  $R$  is the stator resistance,  $\psi_f$  is the flux linkage,  $B$  is the viscous damping coefficient, and  $J$  is the moment of inertia.

### 2.2. Mathematical Model of DPCC

#### 2.2.1. Basic Control Block Diagram of DPCC

Deadbeat is a concept in discrete control systems, which mainly refers to shortening the sampling period for the system to transition to a stable operating state as much as possible, with the ultimate goal of achieving a deadbeat state in the approaching time. The mathematical model in a synchronous rotating coordinate system is discretized to establish the basic DPCC model. Then, online optimization is carried out for current error, the current is adjusted to obtain the current command voltage value, and the voltage command is applied to SVPWM. The basic control block diagram is shown in Figure 1, where  $\omega_m^*$  is the reference mechanical speed,  $i_a$ ,  $i_b$ , and  $i_c$  are the currents of a three-phase stationary frame,  $i_d^*$  and  $i_q^*$  are the reference currents of the  $d$ - and  $q$ - axes,  $i_\alpha$  and  $i_\beta$  are the currents of  $\alpha$ - and  $\beta$ - axes, and  $U_\alpha$  and  $U_\beta$  are the voltages of  $\alpha$ - and  $\beta$ - axes.

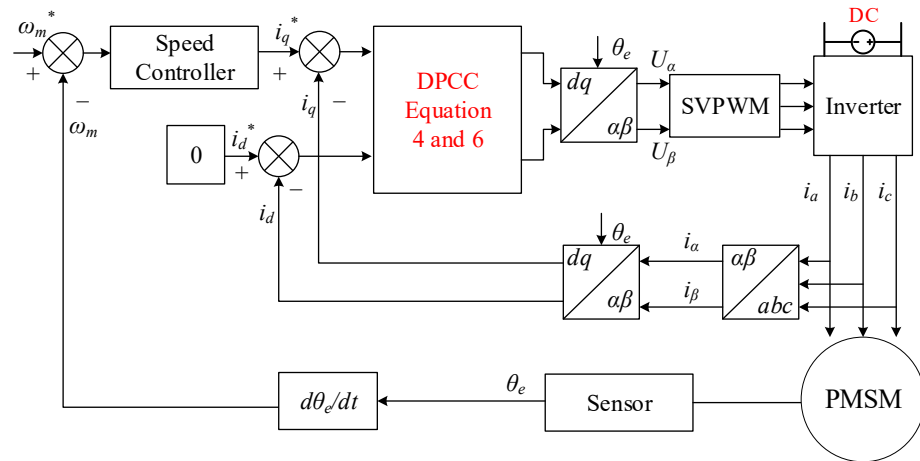


Figure 1. Basic control block diagram of DPCC.

### 2.2.2. Mathematical Model of DPCC

Assuming the control period is short enough and the system is stable at time  $k$ , the forward Euler method is used to discretize the stator voltage equation of PMSM on the  $d$ - $q$  axis in (1) [30], and the  $d$ - $q$  axis current equation at time  $k$  in the discrete state can be obtained as follows:

$$\begin{cases} \frac{(i_{d(k+1)} - i_d)}{T} = -\frac{R}{L}i_{d(k)} + n_p\omega_m i_{q(k)} + \frac{1}{L}u_{d(k)} \\ \frac{(i_{q(k+1)} - i_q)}{T} = -\frac{R}{L}i_{q(k)} - n_p\omega_m i_{d(k)} + \frac{1}{L}u_{q(k)} - \frac{\psi_f n_p \omega_m}{L} \end{cases} \quad (2)$$

where  $T$  is the sampling period.

Equation (2) is transformed to obtain the predicted feedback current for the next time step at time  $k$

$$\begin{cases} i_{d(k+1)} = (1 - \frac{RT}{L})i_{d(k)} + Tn_p\omega_m i_{q(k)} + \frac{T}{L}u_{d(k)} \\ i_{q(k+1)} = (1 - \frac{RT}{L})i_{q(k)} - Tn_p\omega_m i_{d(k)} + \frac{T}{L}u_{q(k)} - \frac{T}{L}\psi_f n_p \omega_m \end{cases} \quad (3)$$

Equation (3) is transformed as

$$i(k+1) = Pi(k) + Qu(k) + X \quad (4)$$

where

$$\begin{cases} i(k) = \begin{bmatrix} i_{d(k)} \\ i_{q(k)} \end{bmatrix}, u(k) = \begin{bmatrix} u_{d(k)} \\ u_{q(k)} \end{bmatrix} \\ P = \begin{bmatrix} 1 - \frac{TR}{L} & Tn_p\omega_m \\ -Tn_p\omega_m & 1 - \frac{TR}{L} \end{bmatrix} \\ Q = \begin{bmatrix} \frac{T}{L} & 0 \\ 0 & \frac{T}{L} \end{bmatrix} \\ X = \begin{bmatrix} 0 \\ -\frac{T}{L}\psi_f n_p \omega_m \end{bmatrix} \end{cases} \quad (5)$$

Due to the sampling period being short, the system samples the signal more frequently and obtains more accurate data, which improves the response speed to signal changes and may reduce errors caused by sampling, and the impact of the sampling period on system stability is ignored. The reference current  $i^*(k)$  is used instead of the  $dq$ -axis current  $i(k+1)$  obtained from the  $k$ -th sampling period. The current error between two different times is seen as the error between the reference current and the feedback current and Equation (4) can be transformed into

$$u(k) = Q^{-1}(i^*(k) - Pi(k) - X) \quad (6)$$

At this point, as long as the error between the given current and the feedback current is based on the same cycle, the voltage command can be accurately calculated. The DPCC model reduces the computational complexity of the system while the complex parameter tuning process is eliminated, which allows the current to quickly track to the specified current.

### 3. DPCC Control System Based on SMO

As mentioned earlier, the DPCC system is susceptible to disturbances, resulting in a decrease in control performance. Based on the insensitivity of sliding-mode control to disturbances and parameters, this section designs a SMO to improve the dynamic quality of motor control systems.

#### 3.1. The Basic Principle of Sliding-Mode Control

Sliding-mode control is a control strategy for variable structure control systems. This control strategy has discontinuity that causes the system structure to change over time. This characteristic allows the system to perform small amplitude, high-frequency up and down movements along a specified trajectory under certain conditions, which is known as sliding mode. This sliding mode is independent of system parameters and disturbances, so it can make the system more robust. In general, nonlinear systems can be represented as

$$\dot{x} = f(x, u, t) \quad (7)$$

$X \in R^n$  and  $u \in R^m$  are the state variable and control variable, respectively. The sliding surface function is as follows:

$$s(x, t), s \in R^m \quad (8)$$

and the controller function

$$u_i(x, t) = \begin{cases} u_i^+(x, t), & s_i(x, t) > 0 \\ u_i^-(x, t), & s_i(x, t) < 0 \end{cases}, i = 1, 2, \dots, m \quad (9)$$

$$u_i^+(x, t) \neq u_i^-(x, t)$$

When the sliding mode exists and all motion points outside of the sliding surface  $s(x, t) = 0$  will reach the sliding surface in a finite time, the conditions for sliding-mode control are satisfied.

#### 3.2. Design of Speed Loop Sliding-Mode Controller

For PMSM, using the rotor magnetic field orientation control method with  $i_d = 0$  can achieve good control results. At this point, Equation (1) can be rewritten as

$$\begin{cases} \frac{di_q}{dt} = \frac{1}{L}(-Ri_q - n_p\psi_f\omega_m + u_q) \\ \frac{d\omega_m}{dt} = \frac{1}{J}(\frac{3}{2}n_p\psi_fi_q - T_L) \end{cases} \quad (10)$$

The state variables of the PMSM system can be defined as

$$\begin{cases} x_1 = \omega_{ref} - \omega_m \\ x_2 = \dot{x}_1 = -\dot{\omega}_m \end{cases} \quad (11)$$

where  $\omega_{ref}$  is the reference speed of the motor, and  $\omega_{mf}$  is the actual speed. According to (10) and (11), it can be inferred that

$$\begin{cases} \dot{x}_1 = -\dot{\omega}_m = \frac{1}{J}(T_L - \frac{3}{2}p\psi_fi_q) \\ \dot{x}_2 = -\ddot{\omega}_m = -\frac{3}{2J}p\psi_f\dot{i}_q \end{cases} \quad (12)$$

(12) can be rewritten as

$$\begin{aligned} \begin{bmatrix} \dot{x}_1 \\ \dot{x}_2 \end{bmatrix} &= \begin{bmatrix} 0 & 1 \\ 0 & 0 \end{bmatrix} \begin{bmatrix} x_1 \\ x_2 \end{bmatrix} + \begin{bmatrix} 0 \\ -D \end{bmatrix} u \\ u &= \dot{i}_q \\ D &= \frac{3}{2} p \psi_f \end{aligned} \quad (13)$$

The sliding surface function is set as

$$s = cx_1 + x_2 \quad (14)$$

where  $c$  is an uncertain parameter. Take the derivative of (14) and one can obtain

$$\dot{s} = c\dot{x}_1 + \dot{x}_2 = cx_2 + \dot{x}_2 = cx_2 - Du \quad (15)$$

In order to achieve better dynamic performance of the motor system, the exponential convergence law is chosen as the control law, and the expression of the controller is

$$u = \frac{1}{D} [cx_2 + \varepsilon \operatorname{sgn}(s) + qs] \quad (16)$$

where  $\varepsilon > 0, q > 0$ .

Thus, the reference current of the  $q$ -axis can be obtained as

$$i_q^* = \frac{1}{D} \int_0^t [cx_2 + \varepsilon \operatorname{sgn}(s) + qs] d\tau \quad (17)$$

According to the sliding mode reachability condition. The stability analysis and proof of the sliding-mode controller are shown as follows.

The Lyapunov function is chosen as  $V = \frac{s^2}{2}$ . Then, the derivative of  $V$  can be written as

$$\begin{aligned} \dot{V} &= ss \\ &= s(-\varepsilon \operatorname{sgn}(s) - qs) \\ &= -\varepsilon s \operatorname{sgn}(s) - qs^2 \\ &= -\varepsilon |s| - qs^2 < 0 \end{aligned} \quad (18)$$

### 3.3. Design of DPCC SMO

When parameter mismatch occurs in the motor current loop, it leads to disturbances in the current loop. In such cases, the voltage equation in the  $dq$ -axis can be expressed as

$$\begin{cases} u_d = L \frac{di_d}{dt} + Ri_d - \omega_e Li_q + \underbrace{(\Delta L \frac{di_d}{dt} + \Delta Ri_d - \omega_e \Delta Li_q)}_{f_d} \\ u_q = L \frac{di_q}{dt} + Ri_q + \omega_e Li_d - \psi_f \omega_e + \underbrace{(\Delta L \frac{di_q}{dt} + \Delta Ri_q - \omega_e \Delta Li_d - \Delta \psi_f \omega_e)}_{f_q} \end{cases} \quad (19)$$

where  $\Delta R$ ,  $\Delta L$ , and  $\Delta \psi_f$  represent the error between the actual and modeled values of resistance, inductance, and flux, respectively.  $f_d$  represents disturbances in the  $d$ -axis parameters, while  $f_q$  represents disturbances in the  $q$ -axis parameters.

In order to improve the parameter robustness of deadbeat, a current loop sliding mode disturbance observer is added to estimate the total disturbance caused by the parameter mismatch in the current loop, and the estimated disturbance is compensated into the prediction model in real time.

The SMO for the current loop disturbances is designed as

$$\begin{cases} u_d = L \frac{d\hat{i}_d}{dt} + R\hat{i}_d - \omega_e L i_q + \hat{f}_d + I_{ds} \\ \frac{d\hat{f}_d}{dt} = k_d I_{ds} \\ u_q = L \frac{d\hat{i}_q}{dt} + R\hat{i}_q + \omega_e L i_d - \psi_f \omega_e + \hat{f}_q + I_{qs} \\ \frac{d\hat{f}_q}{dt} = k_q I_{qs} \end{cases} \quad (20)$$

where  $\hat{i}_d, \hat{i}_q, \hat{f}_d, \hat{f}_q$  are  $d$ -axis current,  $q$ -axis current,  $d$ -axis disturbances, and  $q$ -axis disturbances, respectively.  $I_{ds}, I_{qs}$  are  $dq$ -axis sliding-mode control functions,  $k_d, k_q$  are the sliding-mode control gain of  $dq$ -axis, respectively.

$I_{ds}, I_{qs}$  can be designed as

$$\begin{cases} I_{ds} = -R(\hat{i}_d - i_d) + kL \text{sign}(\hat{i}_d - i_d) \\ I_{qs} = -R(\hat{i}_q - i_q) + kL \text{sign}(\hat{i}_q - i_q) \end{cases} \quad (21)$$

where  $k$  is the positive coefficient.

In order to satisfy the sliding mode stability condition, the sliding-mode control function is required

$$\begin{cases} (\hat{i}_d - i_d) \frac{d(\hat{i}_d - i_d)}{dt} = -\frac{\hat{i}_d - i_d}{L} (R(\hat{i}_d - i_d) + (\hat{f}_d - f_d) + I_{ds}) \leq 0 \\ (\hat{i}_q - i_q) \frac{d(\hat{i}_q - i_q)}{dt} = -\frac{\hat{i}_q - i_q}{L} (R(\hat{i}_q - i_q) + (\hat{f}_q - f_q) + I_{qs}) \leq 0 \end{cases} \quad (22)$$

Then, one can have

$$k > \max\left(\frac{|\hat{f}_d - f_d|}{L}, \frac{|\hat{f}_q - f_q|}{L}\right) \quad (23)$$

When the condition of (23) is satisfied, the SMO is stable.

At this point, a DPCC control system based on SMO can be obtained. Figure 2 shows the dual closed-loop model of SMO-based DPCC studied in this paper. The speed loop is controlled by a sliding-mode controller, which outputs the  $q$ -axis reference current. A sliding-mode observer is used to observe the parameter mismatch ( $\hat{f}_d$ ) and external disturbances ( $\hat{r}_d$ ) generated during motor operation, and it is compensated into DPCC to improve the robustness and anti-interference ability of DPCC.

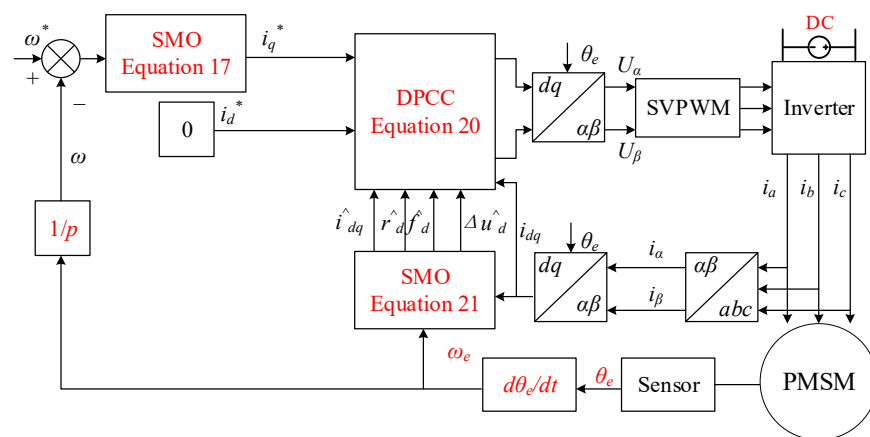


Figure 2. Basic control block diagram of SMO-DPCC.

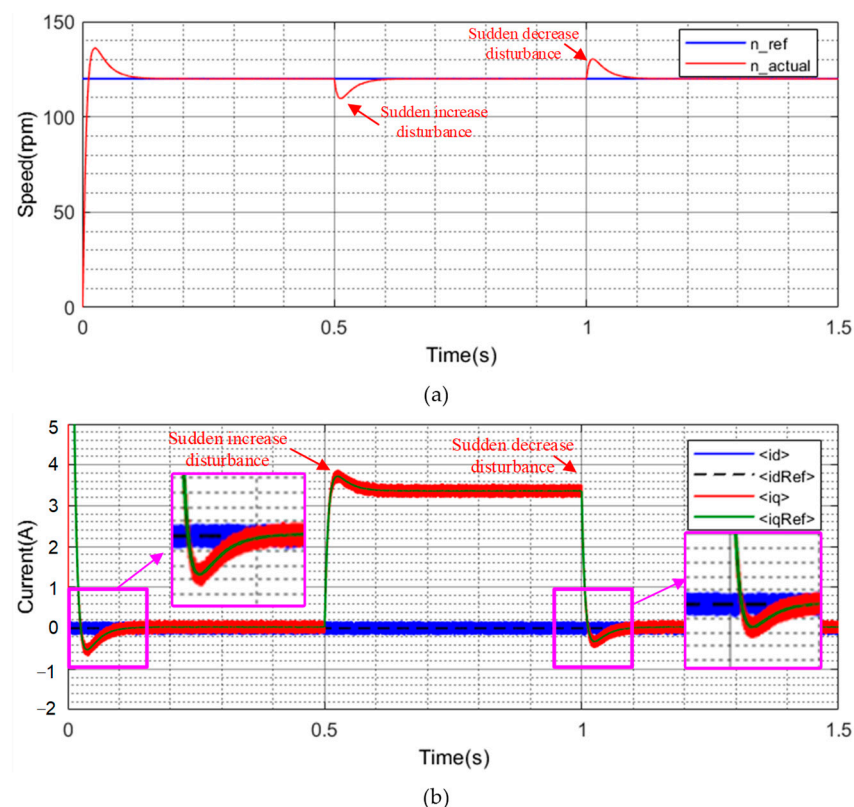
#### 4. Simulation Verification

The built-in Simulink simulation function of MATLAB is used to verify the proposed control system and control method. Due to the susceptibility of DPCC to internal parameter mismatch, the design of simulation experiments is based on parameter mismatch. The parameters used in the simulation are shown in Table 1.

**Table 1.** Simulation parameters and motor parameters.

Parameter	Value	Unit
Rated Power	800	w
Rated Speed	400	rpm
Rated Torque	5	Nm
Rated Voltage	200	V
Rated Current	4	A
Resistance	0.07	$\Omega$
d-axis Inductance	0.625	mH
q-axis Inductance	0.625	mH
Flux	0.1875	Wb
Pole Pairs	5	-
Inertia	0.0008	Kg·m <sup>2</sup>
Sampling Frequency	10	kHz
Sliding Mode Gain	300	
LPF Cut-off Frequency	2000	Hz
ESO Parameters	$\beta_1 = 1.5, \beta_2 = 700$	
AO Parameters	$\alpha_c = 1$	

In the speed loop, a 5 Nm load surge perturbation is applied at 0.5 s and a 5 Nm load surge decrease perturbation is applied at 1 s. The inductance, resistance, and flux of the model are set to 0.5 times the nominal values, a delay of  $1 \times 10^{-4}$  s is also added in the simulation, and the simulation results are shown in Figure 3.

**Figure 3.** Simulation result of SMO-DPCC. (a) Speed waveform. (b) Current waveform.

From Figure 3, it can be seen that the motor can still operate effectively even in the case of mismatched key parameters. When increasing or decreasing the load on the motor, the motor has a small overshoot, and the current tracking is stable, which means less affected by internal and external disturbances.

In order to better demonstrate the control effect of the proposed method, the extended state observer (ESO) proposed in [31] and adaptive observer (AO) proposed in [32] are applied for observation and comparison. The same control conditions and interference are set, and the simulation results are shown in Figures 4 and 5.

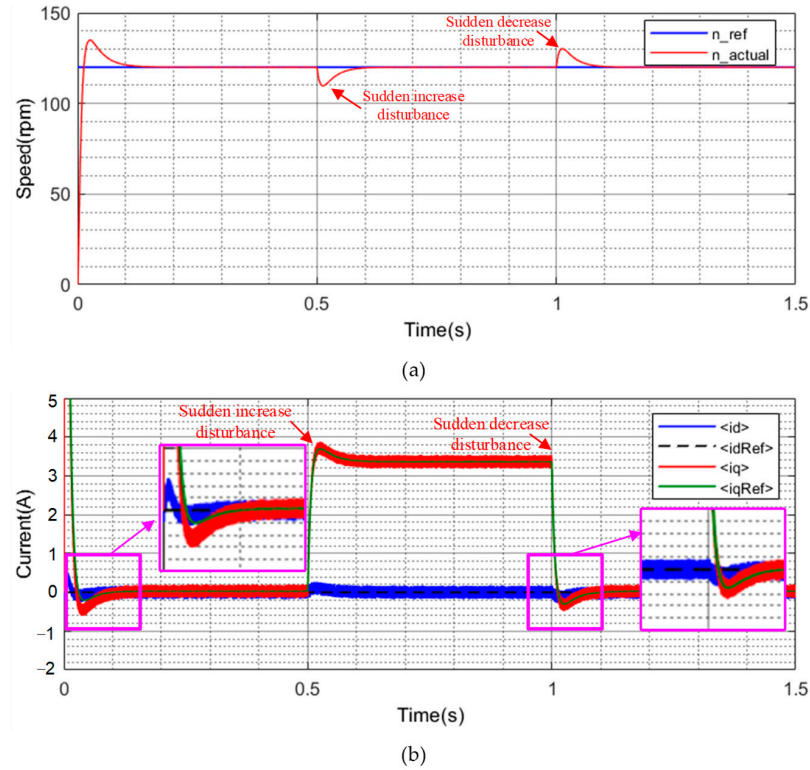


Figure 4. Simulation result of ESO-DPCC. (a) Speed waveform. (b) Current waveform.

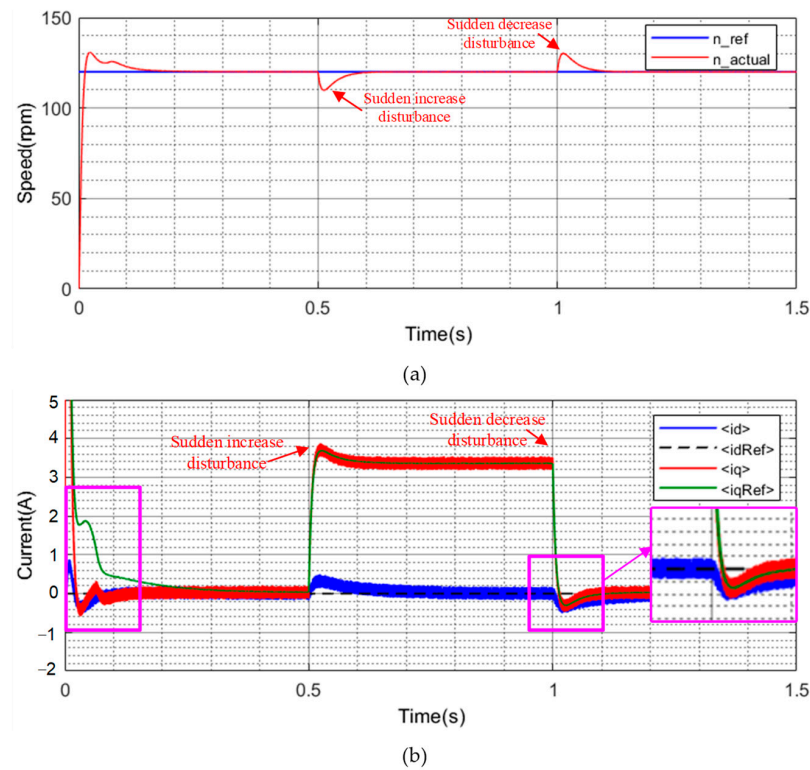
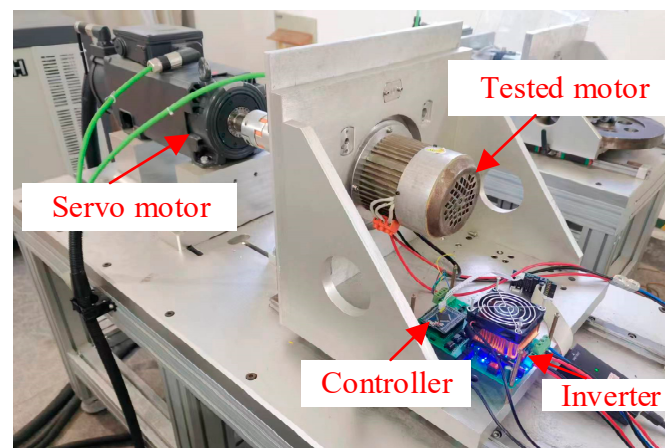


Figure 5. Simulation result of AO-DPCC. (a) Speed waveform. (b) Current waveform.

From the comparative simulation results, it can be seen that the three are relatively consistent in terms of speed performance, and all have good performance. From the perspective of current tracking, it can be seen that the AO-DPCC method has the worst current tracking performance, while the current tracking method proposed in this article is more stable and has obvious advantages. This is because the method proposed in this article is mainly applied to the current loop, which aims to improve the current tracking performance.

## 5. Experimental Results

In this section, the experimental platform is established and a surface-mounted PMSM is selected as a prototype for control experiments to verify the effectiveness of the proposed algorithm. The experimental platform is shown in Figure 6.



**Figure 6.** The experimental platform.

The drive system of the motor is designed, and the control algorithm is implemented using STM32 code. The program is written in C language and developed using Keil-uVision5 software. The circuit in this article is mainly designed based on Intelligent Power Module (IPM), using Mitsubishi Electric's PSS15S92F6 module as a three-phase inverter. This section uses STM32F407VET of the ARM company based on the Cortex-M4 processor core as the control chip. The inductance, resistance, and flux of the model are set to 0.5 times the nominal values. The sampling period used in the controller is 10 kHz. The relevant parameters of the motor are shown in Table 1. Experiments are conducted at low speeds of 60 rpm and medium speeds of 120 rpm, respectively.

### 5.1. The Experiment at 60 rpm

Motor experiments are conducted at a speed of 60 rpm to verify the effectiveness of the proposed algorithm. The experimental results are shown in Figure 7.

From Figure 7, it can be seen that after giving the current command, the control algorithm responded quickly. At the 10th second, commands to increase and decrease the current are given in Figures 7a and 7b, respectively, and the control objectives can be implemented after about 0.1 s. From Figure 7, it can also be seen that the current jitter of the motor is small and has a good current performance.

In order to demonstrate the superiority of the proposed algorithm, comparative experiments are conducted in this article. ESO and AO are applied for observation and comparison.

It can be seen that the combination of ESO with DPCC also has good control effects, but the response time and current curve jitter are worse than the proposed control scheme. Table 2 provides a more intuitive demonstration of the experimental results.

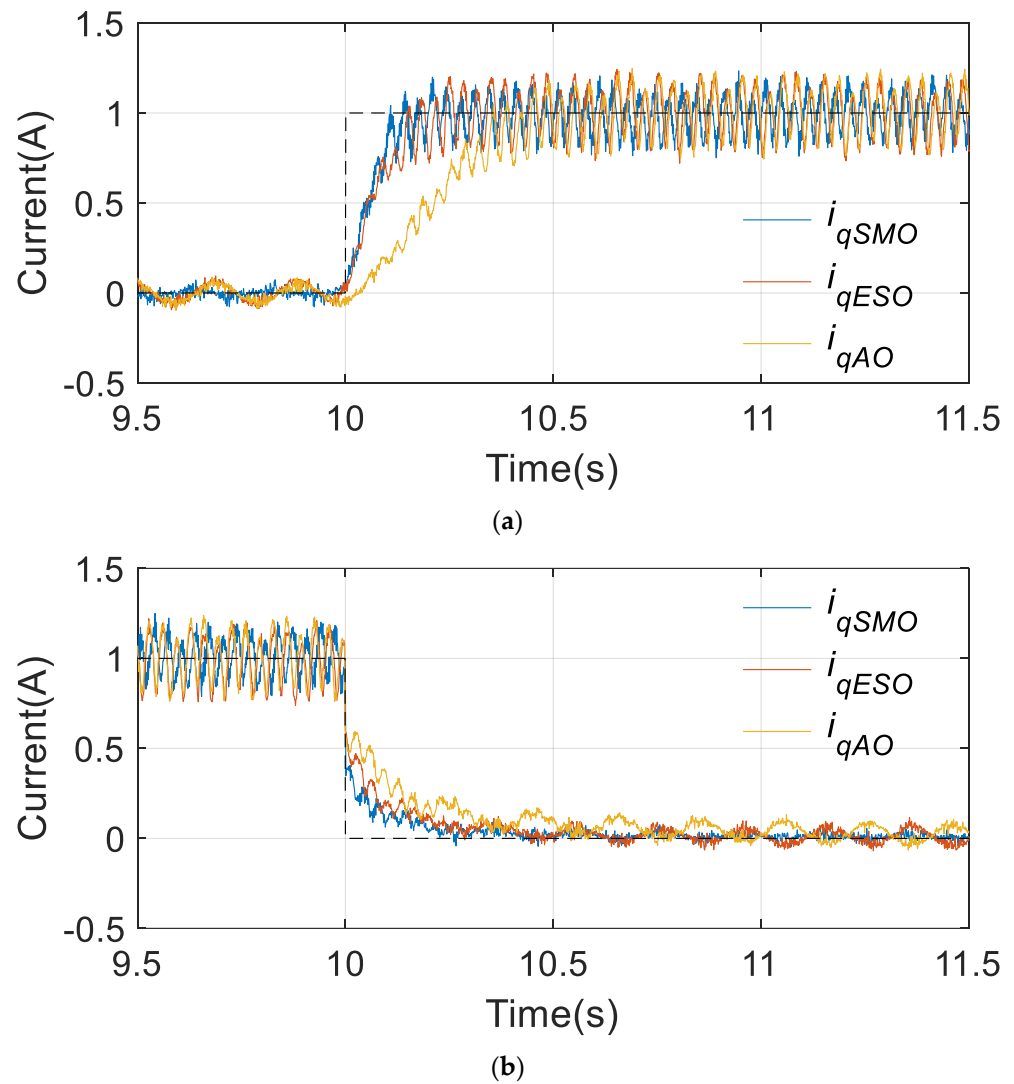


**Figure 7.** Response time comparison of three schemes under 60 rpm. (a) Current sudden increase. (b) Current sudden decrease.

**Table 2.** Comparison of the effects of different control schemes at 60 rpm.

Schemes	Response Time at Increasing	Response Time at Decreasing
SMO-DPCC	0.111 s	0.3871 s
ESO-DPCC	0.16 s	0.889 s
AO-DPCC	0.36 s	0.602 s

Table 2 shows that the SMO-DPCC proposed in this paper shows the best results when, in the current surge, its rise time is about 0.111 s, while the rise time of ESO-DPCC and AO-DPCC is slightly longer because the synovial observer designed in this paper has faster disturbance identification speed. However, the decreased time SMO-DPCC shows a greater advantage. From the perspective of  $d$ - $q$  axis current performance, SMO has the best ability to observe periodic disturbances, and the  $d$ - $q$  axis current under ESO and AO methods has obvious periodic fluctuations.

### 5.2. The Experiment at 120 rpm

The performance of the proposed method is also validated under medium-speed conditions. Three methods are also used for verification, and the experimental results are shown in Figure 8.

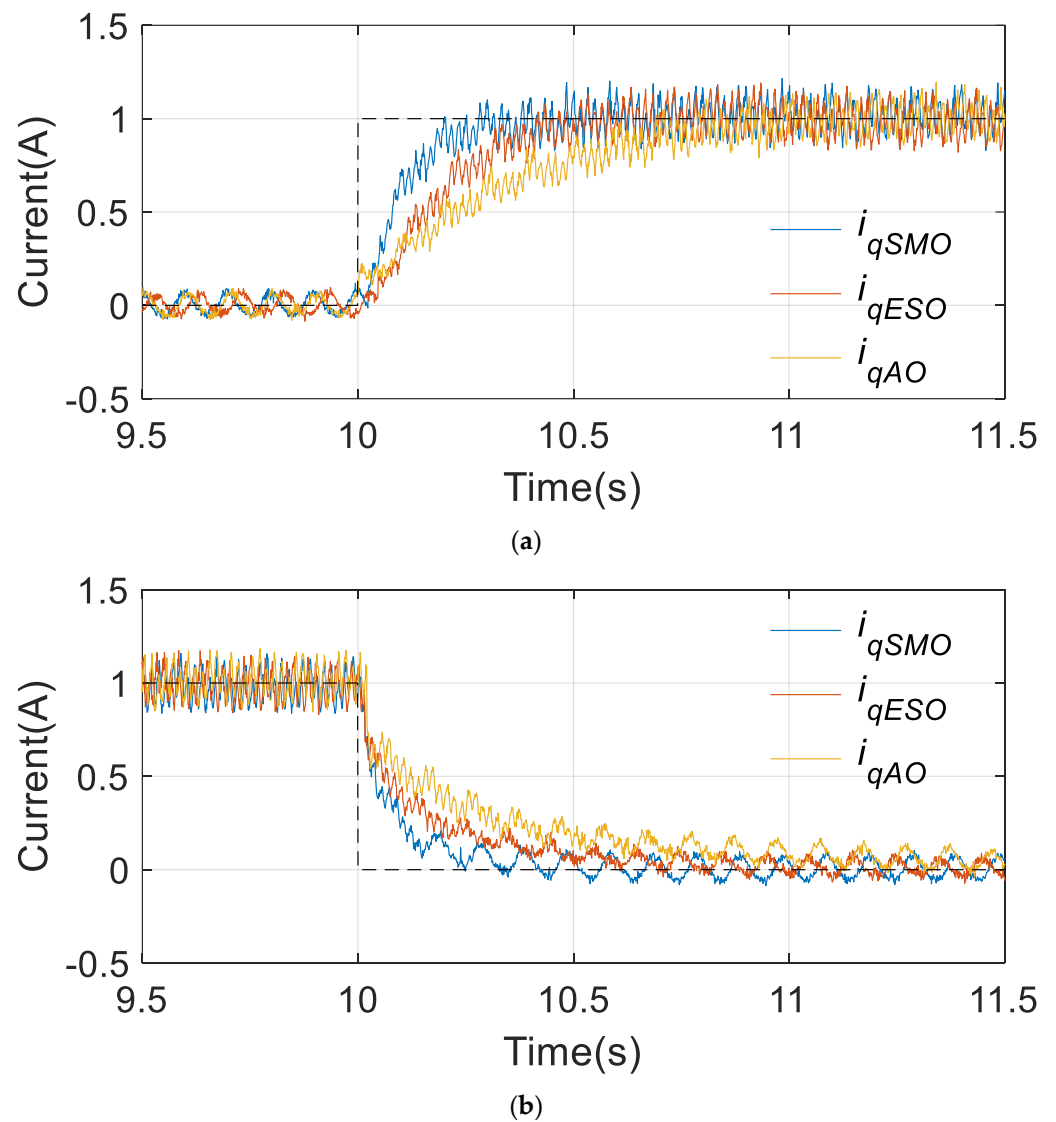


**Figure 8.** Response time comparison of three schemes under 120 rpm. (a) Current sudden increase. (b) Current sudden decrease.

It can be seen that there is significant distortion in the current waveform after using the other two methods. ESO-DPCC exhibits significant current jitter and significantly longer response time in terms of current jitter. AO-DPCC performs the worst among the three. The specific comparison of the three is shown in Table 3.

**Table 3.** Comparison of the effects of different control schemes at 120 rpm.

Schemes	Response Time at Increasing	Response Time at Decreasing
SMO-DPCC	0.16 s	0.7911 s
ESO-DPCC	0.3901 s	1.0321 s
AO-DPCC	0.6511 s	1.8731 s

When the motor speed is increased to 120 rpm, the current of the d-q axis under the three schemes shows a certain disturbance. At the same time, with the increase in the speed, the disturbance caused by the parameter mismatch is also greater, and the current response time of the three schemes is also prolonged, but SMO-DPCC still has the optimal response speed.

### 5.3. Effect of Temperature Rise at 60 rpm

In our experimental setup, the motor operated for 3 h, with the ambient temperature maintained at approximately 19.4 degrees Celsius. Following this period, the surface temperature of the motor rose to approximately 41.2 degrees Celsius. Under these conditions, experimental procedures adhered to the rated parameters of the motor, facilitating the validation of algorithmic efficacy amidst parameter mismatch. At 60 rpm, we selected the most representative experiment and tested the dq axes currents response waveform under the q-axis reference current mutation from 1 A to 0 A, as shown in Figure 9.

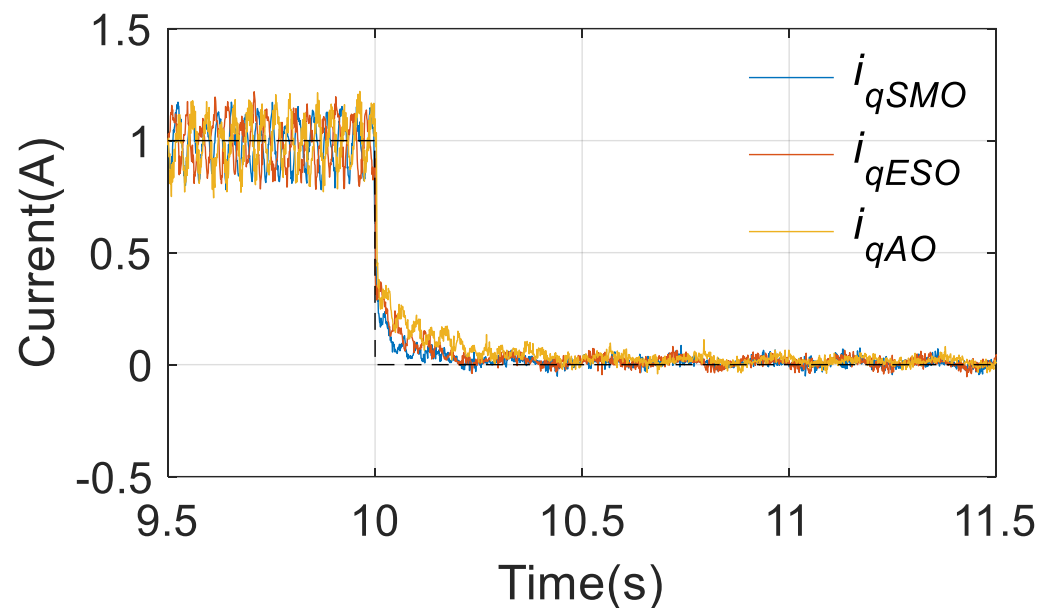


**Figure 9.** Comparison of d-q axis current.

It can be seen that the strategy recommended in this paper has the best effect both in the steady-state fluctuation under 1A and in the response speed of the current mutation. Compared with the previous experimental results of inductance, resistance, and flux at 0.5 times the standard value, the effect of temperature change on the motor performance is slightly smaller. The experimental results fully verify the effectiveness and superiority of the algorithm proposed in this paper.

## 6. Conclusions

In this article, a new DPCC method based on SMO is proposed. A sliding-mode observer is designed based on the DPCC model and the basic equations of the motor and applied to the current loop of the motor control system. The addition of SMO enables accurate and fast observation of disturbances in the current loop, including but not limited to disturbances caused by parameter mismatch. The effectiveness and disturbance rejection performance of the proposed method are verified based on simulation models. The superiority of the proposed method is verified through experimental platforms and comparative experiments, and both the response speed and the control accuracy have been greatly improved.

**Author Contributions:** Z.Z. implemented the research, performed the analysis, and wrote the paper. Y.W. collated simulation data. Q.X. was responsible for guidance and manuscript editing. All authors have read and agreed to the published version of the manuscript.

**Funding:** This research was funded in part by the special fund of Jiangsu Province for the transformation of scientific and technological achievements (No. BA2023048), the Research Program Key Project of the Anhui Higher Education Institutions of China under Grant 2022AH051085, and the

Top Talents Academic Support Project of the Anhui Provincial Department of Education University Discipline (Major) of China under Grant gxbjZD2020088.

**Institutional Review Board Statement:** Not applicable.

**Informed Consent Statement:** Not applicable.

**Data Availability Statement:** Data are contained within the article.

**Conflicts of Interest:** The authors declare no conflicts of interest.

## References

1. Cavus, B.; Aktas, M. MPC-Based flux weakening control for induction motor drive with DTC for electric vehicles. *IEEE Trans. Power Electron.* **2022**, *38*, 4430–4439. [[CrossRef](#)]
2. Zhang, D.; Zhang, H.; Li, X.; Zhao, H.; Zhang, Y.; Wang, S.; Ahmad, T.; Liu, T.; Shuang, F.; Wu, T. A PMSM Control system for electric vehicle using improved exponential reaching law and proportional resonance theory. *IEEE Trans. Veh. Technol.* **2023**, *72*, 8566–8578. [[CrossRef](#)]
3. Liu, Z.; Huang, X.; Hu, Q.; Li, Z.; Jiang, Z.; Yu, Y.; Chen, Z. A Modified deadbeat predictive current control for improving dynamic performance of PMSM. *IEEE Trans. Power Electron.* **2022**, *37*, 14173–14185. [[CrossRef](#)]
4. Lin, C.-K.; Liu, T.-H.; Yu, J.-T.; Fu, L.-C.; Hsiao, C.-F. Model-Free Predictive Current Control for Interior Permanent-Magnet Synchronous Motor Drives Based on Current Difference Detection Technique. *IEEE Trans. Ind. Electron.* **2014**, *61*, 667–681. [[CrossRef](#)]
5. Dong, Z.; Song, Z.; Wang, W.; Liu, C. Improved zero-sequence current hysteresis control-based space vector modulation for open-end winding PMSM drives with common DC bus. *IEEE Trans. Ind. Electron.* **2022**, *70*, 10755–10760. [[CrossRef](#)]
6. Xue, Y.; Meng, D.; Yin, S.; Han, W.; Yan, X.; Shu, Z.; Diao, L. Vector-based model predictive hysteresis current control for asynchronous motor. *IEEE Trans. Ind. Electron.* **2019**, *66*, 8703–8712. [[CrossRef](#)]
7. Ruan, Z.; Song, W.; Zhao, L.; Zhang, Y.; Guo, Y. A variable switching frequency space vector pulse width modulation control strategy of induction motor drive system with torque ripple prediction. *IEEE Trans. Energy Convers.* **2023**, *38*, 993–1003. [[CrossRef](#)]
8. Nguyen, M.-K.; Choi, Y.-O. PWM control scheme for quasi-switched-boost inverter to improve modulation index. *IEEE Trans. Power Electron.* **2018**, *33*, 4037–4044. [[CrossRef](#)]
9. Shan, Y.; Hu, J.; Chan, K.W.; Islam, S. A Unified Model Predictive Voltage and Current Control for Microgrids With Distributed Fuzzy Cooperative Secondary Control. *IEEE Trans. Ind. Inform.* **2021**, *17*, 8024–8034. [[CrossRef](#)]
10. Gao, S.; Yuan, L.; Dai, Y.; Mou, D.; Chen, K.; Zhao, Z. High-Frequency Current Predictive Control Method for Multiactive-Bridge Converter. *IEEE Trans. Power Electron.* **2022**, *37*, 10144–10148. [[CrossRef](#)]
11. Wang, J.; Wang, F.; Wang, G.; Li, S.; Yu, L. Generalized proportional integral observer-based robust finite control set predictive current control for induction motor systems with time-varying disturbances. *IEEE Trans. Ind. Inform.* **2018**, *14*, 4159–4168. [[CrossRef](#)]
12. Gao, J.; Gong, C.; Li, W.; Liu, J. Novel compensation strategy for calculation delay of finite control set model predictive current control in PMSM. *IEEE Trans. Ind. Electron.* **2019**, *67*, 5816–5819. [[CrossRef](#)]
13. Sun, Z.; Deng, Y.; Wang, J.; Yang, T.; Wei, Z.; Cao, H. Finite control set model-free predictive current control of PMSM with two voltage vectors based on ultralocal model. *IEEE Trans. Power Electron.* **2022**, *38*, 776–788. [[CrossRef](#)]
14. Liu, Q.; Hameyer, K. Torque ripple minimization for direct torque control of PMSM with modified FCSMPC. *IEEE Trans. Ind. Appl.* **2016**, *52*, 4855–4864. [[CrossRef](#)]
15. Chen, W.; Zeng, S.; Zhang, G.; Shi, T.; Xia, C. A Modified double vectors model predictive torque control of Permanent magnet synchronous motor. *IEEE Trans. Power Electron.* **2019**, *34*, 11419–11428. [[CrossRef](#)]
16. Petkar, S.G.; Eshwar, K.; Thippiripati, V.K. A Modified model predictive current control of permanent magnet synchronous motor drive. *IEEE Trans. Ind. Electron.* **2020**, *68*, 1025–1034. [[CrossRef](#)]
17. Ke, D.; Wang, F.; Yu, X.; Davari, S.A.; Kennel, R. Predictive error model-based enhanced observer for PMSM deadbeat control systems. *IEEE Trans. Ind. Electron.* **2023**, *71*, 2242–2252. [[CrossRef](#)]
18. Xu, Y.; Li, S.; Zou, J. Integral sliding mode control based deadbeat predictive current control for PMSM drives with disturbance rejection. *IEEE Trans. Power Electron.* **2021**, *37*, 2845–2856. [[CrossRef](#)]
19. Gao, F.; Yin, Z.; Li, L.; Li, T.; Liu, J. Gaussian noise suppression in deadbeat predictive current control of permanent magnet synchronous motors based on augmented fading kalman filter. *IEEE Trans. Energy Convers.* **2022**, *38*, 1410–1420. [[CrossRef](#)]
20. Yang, J.; Su, J.; Li, S.; Yu, X. High-Order Mismatched Disturbance Compensation for Motion Control Systems Via a Continuous Dynamic Sliding-Mode Approach. *IEEE Trans. Ind. Inform.* **2013**, *10*, 604–614. [[CrossRef](#)]
21. Yang, J.; Chen, W.-H.; Li, S. Non-linear disturbance observer-based robust control for systems with mismatched disturbances/uncertainties. *IET Control Theory Appl.* **2011**, *5*, 2053–2062. [[CrossRef](#)]
22. Yang, H.; Li, X.; Chen, Z.; Yin, S. A Novel adaptive observer-based fault reconstruction and state estimation method for markovian jump systems. *IEEE Syst. J.* **2020**, *15*, 2305–2313. [[CrossRef](#)]

23. Zhang, H.; Zhang, W. Incremental quadratic constrained nonlinear adaptive reduced-order observer and its application to chaos synchronization. In Proceedings of the 2019 3rd International Conference on Electronic Information Technology and Computer Engineering (EITCE), Xiamen, China, 18–20 October 2019; pp. 767–770.
24. Du, C.; Yin, Z.; Liu, J.; Zhang, Y.; Sun, X. A Speed Estimation Method for Induction Motors Based on Active Disturbance Rejection Observer. *IEEE Trans. Power Electron.* **2020**, *35*, 8429–8442. [[CrossRef](#)]
25. Yao, H.; Wu, J.; Xi, J.; Wang, L. Active disturbance rejection controller based time-varying formation tracking for second-order multi-agent systems with external disturbances. *IEEE Access* **2019**, *7*, 153317–153326. [[CrossRef](#)]
26. Mi, Y.; Song, Y.; Fu, Y.; Wang, C. The adaptive sliding mode reactive power control strategy for wind–diesel power system based on sliding mode observer. *IEEE Trans. Sustain. Energy* **2019**, *11*, 2241–2251. [[CrossRef](#)]
27. Deng, H.; Li, Q.; Chen, W.; Zhang, G. High-Order Sliding Mode Observer Based OER Control for PEM Fuel Cell Air-Feed System. *IEEE Trans. Energy Convers.* **2017**, *33*, 232–244. [[CrossRef](#)]
28. Guo, X.; Huang, S.; Lu, K.; Peng, Y.; Wang, H.; Yang, J. A fast sliding mode speed controller for pmsm based on new compound reaching law with improved sliding mode observer. *IEEE Trans. Transp. Electrification* **2022**, *9*, 2955–2968. [[CrossRef](#)]
29. Xudong, L.; Ke, L.; Qi, Z.; Chenghui, Z. Single-loop predictive control of permanent magnet synchronous motor based on nonlinear disturbance observe. In Proceedings of the Chinese Society of Electrical Engineering, Guangzhou, China, 6–9 November 2018; Volume 38, pp. 2153–2162+2230.
30. Fang, H.; Duan, X.; Yang, Y.; Wang, Y.; Luo, G. Deadbeat Control of Permanent Magnet Synchronous Motor Based on MRAS Parameter Identification. In Proceedings of the 2020 23rd International Conference on Electrical Machines and Systems (ICEMS), Hamamatsu, Japan, 24–27 November 2020.
31. Wu, S.; Shi, J.; Li, Z. Research on Deadbeat Predictive Current Control of PMSM Based on ESO. *Electr. Drive* **2021**, *51*, 22–28.
32. Chen, J.; Fan, Y.; Chen, Q. Model-free deadbeat predictive current control of NIPMVMs considering dead-time effect. *J. Power Electron.* **2024**, 1–9. [[CrossRef](#)]

**Disclaimer/Publisher’s Note:** The statements, opinions and data contained in all publications are solely those of the individual author(s) and contributor(s) and not of MDPI and/or the editor(s). MDPI and/or the editor(s) disclaim responsibility for any injury to people or property resulting from any ideas, methods, instructions or products referred to in the content.